

Precipitates effect on microstructure of as-deformed and as-annealed AZ41 magnesium alloys by adding Mn and Ca

Shouren Wang · Ru Ma · Liying Yang ·
Yong Wang · Yanjun Wang

Received: 9 October 2010 / Accepted: 9 December 2010 / Published online: 30 December 2010
© Springer Science+Business Media, LLC 2010

Abstract The microstructure and precipitates effect of AZ41 alloys by adding Mn and Ca during hot compression ($300\text{ }^{\circ}\text{C}/0.1\text{ s}^{-1}$) followed by annealing ($300\text{ }^{\circ}\text{C}/1000\text{ s}$) have been studied. A kind of bimodal structure consist of a large fraction of the original and deformed grains as well as a small fraction of newly formed grains is found in as-deformed alloys. Equiaxed and fine-grained microstructures occur in as-annealed samples. For Mn-free and Ca-free alloys, Zener pinning effect is minor. Particle stimulated nucleation promotes recrystallization. For Mn- and Ca-containing alloys, fine particles retard dislocation glide forming high density dislocation to inhibit recrystallization.

Introduction

It is inevitable that alloying in magnesium certainly result in occurrence of amount of second-phase particles and precipitates. The second-phase particles can alter the textures developed during thermomechanical processing and manipulate grain size by influencing recrystallization [1]. Particles can either promote or suppress recrystallization depending on their size, spacing, and fraction [2]. The Zener pinning drag mechanism (ZPD) describes the finely dispersed second-phase particles pinning the subgrains, preventing extensive grain growth, and improving grain/grain misorientation density. However, the particle stimulated nucleation (PSN) describes the larger, widely spaced particles promoting recrystallization, and manipulating the texture. Robson et al. [1] discussed the influence of large

particles ($>1\text{ }\mu\text{m}$ diameter) on the recrystallization behavior of magnesium alloys deformed in plane strain compression. Lee et al. [3] have studied role of the icosahedral phase (I-phase) particles on the improved mechanical properties of Mg-Zn-Y alloys. Mendis et al. [4] has researched the effect of precipitation on mechanical properties of Mg-Zn-Zr alloys. However, there are little researches to discuss the effect of PSN and ZPD at the same time. One of purposes in this study was to discuss particles effect on microstructure of AZ41M ($\text{Mg}-4.1\text{Al}-1.2\text{Zn}-0.5\text{Mn}-0.5\text{Ca}$, “M” denotes the modification of base material by adding Mn and Ca elements) magnesium alloy. Manganese is added to the AZ series alloys primarily to improve corrosion resistance, to refine the as-cast grain size, and also to control Fe content by precipitating Fe-Mn compound [5]. Ca is the promising element not only because of its low density and low cost, but also because of its improving properties for practical applications. Therein, Ca can evidently refine grain due to the formation of a thermally stable second phase such as $(\text{Mg}, \text{Al})_2\text{Ca}$, Mg_2Ca , or Al_2Ca . Furthermore, Ca addition significantly improves the elevated temperature properties and corrosion resistance of magnesium alloys [6].

Experimental procedure

The alloy used in this study is commercial magnesium alloy AZ41M (“M” indicated as modified), which chemical compositions were shown in Table 1. The ingot was homogenized at $400\text{ }^{\circ}\text{C}$ for 20 h, and then machined into a block with a size of $50 \times 20 \times 3\text{ mm}^3$. The homogenized samples were deformed using an Instron 4505 compression testing machine. Uniaxial compression tests were performed under the temperature of $300\text{ }^{\circ}\text{C}$ and strain rates of 0.1 s^{-1} .

S. Wang (✉) · R. Ma · L. Yang · Y. Wang · Y. Wang
School of Mechanical Engineering, University of Jinan,
Ji’nan 250022, China
e-mail: sherman0158@tom.com

Table 1 Chemical composition of AZ41M alloys (wt%)

Alloy	Al	Zn	Mn	Ca	Fe	Si	Mg
AZ41M	4.2	1.2	0.5	0.5	0.010	0.002	Bal.

The specimens were quenched by nitrogen gas immediately after hot compression to preserve the microstructure in its as-deformed state. And then, the samples were annealed at temperature of 300 °C and time of 1000 s. The annealed samples were mechanically polished with polycrystalline diamond suspension glycol-based solution. The grain structure was revealed by subsequent etching in 7 s with a solution of picric acid (5 g), acetic acid (5 mL), distilled water (10 mL), and ethanol (100 mL). The average grain size was analyzed by image analyzer. Microstructural evolution and grain-boundary distribution measurements were performed by electron backscatter diffraction (EBSD). The EBSD specimens were prepared using mechanical polishing and electro polishing. The mechanical polishing was done using 2000# sand paper. The electro polishing was done at 11 V for 120 s in a solution of 400 mL butyl glycol, 80 mL ethanol, and 40 mL perchloric acid (HClO_4) under 15 °C in

order to remove surface strain. EBSD data was acquired using JEOL JSM-7001F field emission scanning electron microscope (FESEM) and HKL Channel 5 EBSD software (HKL Technology, Denmark). The FESEM was operated at 20 kV in high vacuum mode and the specimen was tilted at 70°. Precipitates were examined by using a JEM-2100F transmission electron microscope (TEM) operating at 200 kV. Thin foils were prepared by a twin jet electro-polisher using a solution of HNO_3 (10%), glycerin (30%), and methanol (60%). Finally, the thin foils were ion-beam milled. Selected area diffraction patterns were taken from regions having diameter of 3 μm . Quantitative analysis was carried out using energy dispersive spectroscopy (EDS).

Results and discussion

Microstructure changes of AZ41M alloys under different conditions are shown in Fig. 1. Figure 1a shows the microstructure of AZ41M alloys in as-casted state. It consists of approximately equiaxed grains (80–120 μm) and some second precipitated phases along the grain boundary, and the interior of the grains. It contains large

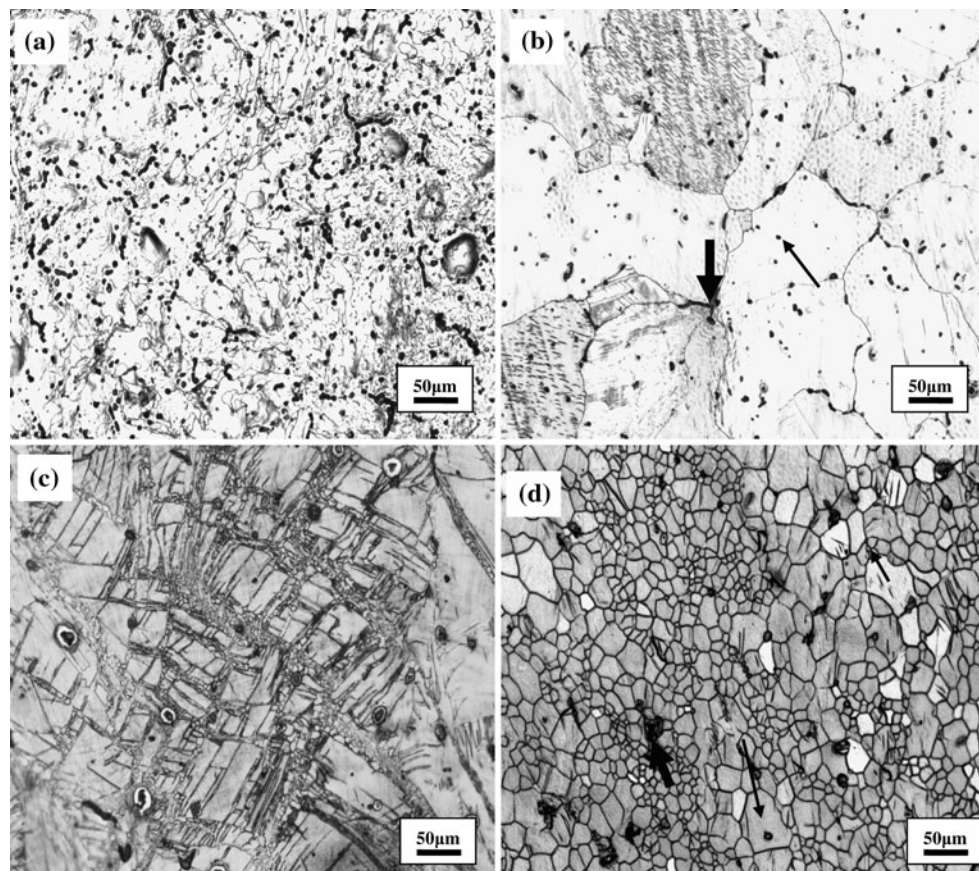


Fig. 1 Optical microstructure of AZ41M alloys under different conditions: **a** as-casted state, **b** as-homogenized state, **c** as-deformed state, and **d** as-annealed state

($>1\text{ }\mu\text{m}$ diameter) and small ($\leq 1\text{ }\mu\text{m}$ diameter) particles. The measured volume fraction of particles in AZ41M alloy was 15.3%. Figure 1b shows the microstructure of AZ41M alloys in as-homogenized state. It is shown that grain size (100–200 μm) turns bigger compared with as-casted structure, and lots of particles have been dissolved into matrix by homogenization though parts of them are still observed. Some small particles distribute in the interior of the grains (indicated by fine line arrows). A cluster of large segregated particles are studded at grain triple junctions (indicated by thick line arrows). The grain boundaries turn more clearly. The measured volume fraction of particles is 11.9%. Figure 1c shows the microstructure changes of AZ41M alloys under uniaxial hot compression conditions. It can be seen that a kind of distinct bimodal structure consisting a large fraction of the original and deformed grains, and a small fraction of newly formed grains is observed. The coarse as-casted structure has been replaced by heterogeneous deformed structures. Shear bands are observed on the bimodal structure. Amount of fine recrystallized grains distribute in the shear bands. Deformation twins are extensive. Some fine DRXed grains can also be observed at the twinned regions. These significant microstructural changes indicated that hot compression processing is effective in refining grain size. Optical micrographs show the typical features after annealing for 1000 s under 300 °C (Fig. 1d). It exhibits an equiaxed and fine-grained microstructure which indicates that homogeneous nucleation and grain growth occurred during static recrystallization (SRX). And that, some fine necklace DRXed grains along the prior grain boundaries and within shear bands. Some globular particles are still found to be located on the grain boundaries or embedded interior of the grain. Amount of fine particles ($\leq 1\text{ }\mu\text{m}$ diameter) and several large particles ($>1\text{ }\mu\text{m}$ diameter) are observed. The volume fraction and the average radius of fine particles are 4.1% and 0.6 μm , respectively. The volume fraction and the average radius of large particles are 8.9% and 2.0 μm , respectively.

Figure 2a, b show the crystal orientation map of the as-deformed and as-annealed specimen. Orientation color code is given for the hexagonal system. The similar color of the grains denotes the smaller misorientation angle. The different colors represent different orientations of the grains. From Fig. 2a, a bimodal structure consisting long elongated grains and dynamic recrystallized grains has been observed. A strong basal textures lead to the *c*-axis aligned in the plane normal direction (ND) of the sample. From Fig. 2b, some long elongated grains are still observed (black arrow). Fine equiaxed grains (circle) and large secondary recrystallized grains referred as static annealed grains (white arrow) are also observed. To investigate texture evolution during annealing, EBSD measurements

are carried out along the ND. As-deformed samples possessed a strong basal texture, which causes the *c*-axis aligned in the ND. Annealing at 300 °C for 1000 s leads to changes in both basal and non-basal textures. The distribution of misorientation angles in the as-deformed and as-annealed specimen are shown in Fig. 2c. The frequency of low angle grain boundaries (LAGBs) with misorientation angles below 15° in as-deformed samples are 22.1%. The recrystallized grain fraction is 12.7% calculated by EBSD method. The substructured grain fraction is 10%. Large numbers of as-deformed grains (77.3%) are observed. The majority of grain boundaries in the microstructure are high angle grain boundaries (HAGBs, with misorientation angles beyond 15°) and the frequency of HAGBs is 55.6% in as-annealed sample. Figure 2d shows the TEM micrograph of as-annealed sample. It is seen that some fine precipitates as $\beta\text{-Mg}_{17}\text{Al}_{12}$, Al_8Mn_5 , and Al_2Ca can be seen. The morphology of $\beta\text{-Mg}_{17}\text{Al}_{12}$ phase is lamellar, which distributes at grain boundaries. Some Ca element dissolves into $\beta\text{-Mg}_{17}\text{Al}_{12}$ phase resulting in its refinement and improvement of its thermal stability. Several literatures [7–9] have reported that adding small amount of Ca to magnesium alloy can change the morphology of $\beta\text{-Mg}_{17}\text{Al}_{12}$ phase at grain boundaries and improve the thermal stability of $\beta\text{-Mg}_{17}\text{Al}_{12}$ phase. By EDS, the Al–Mn intermetallic is identified as Al_8Mn_5 with D8₁₀ structure. The at% concentrations calculated from this spectrum are 60.8% for Al and 39.2% for Mn. They correspond to an Al/Mn ratio of 1.6. The morphology of Al_8Mn_5 intermetallics is nearly round. Therein, amount of new fine precipitates indicated as $\text{A1}_2\text{Ca}$ phase with C15 structure are stable in the equilibrium condition by computational thermodynamics and experimental investigations.

Large particles promoting recrystallization and fine particles pinning boundary migration are well known and widely observed in magnesium alloys. The grain-boundary migration rate depends on the balance between the driving and the pinning forces due to curvature grain-boundary radius and precipitates, respectively. A grain boundary cannot move if the driving force is less than the pinning one even it has a high mobility [10]. It is well known that the grain growth stops when the matrix mean grain size *R* achieves the limiting value as [11],

$$R = \frac{4r}{3f} \quad (1)$$

where *f* and *r* are the volume fraction and the average radius of pinning particles, respectively.

The driving force is described as,

$$P = 2\frac{\gamma}{R} \quad (2)$$

where γ is the grain-boundary energy.

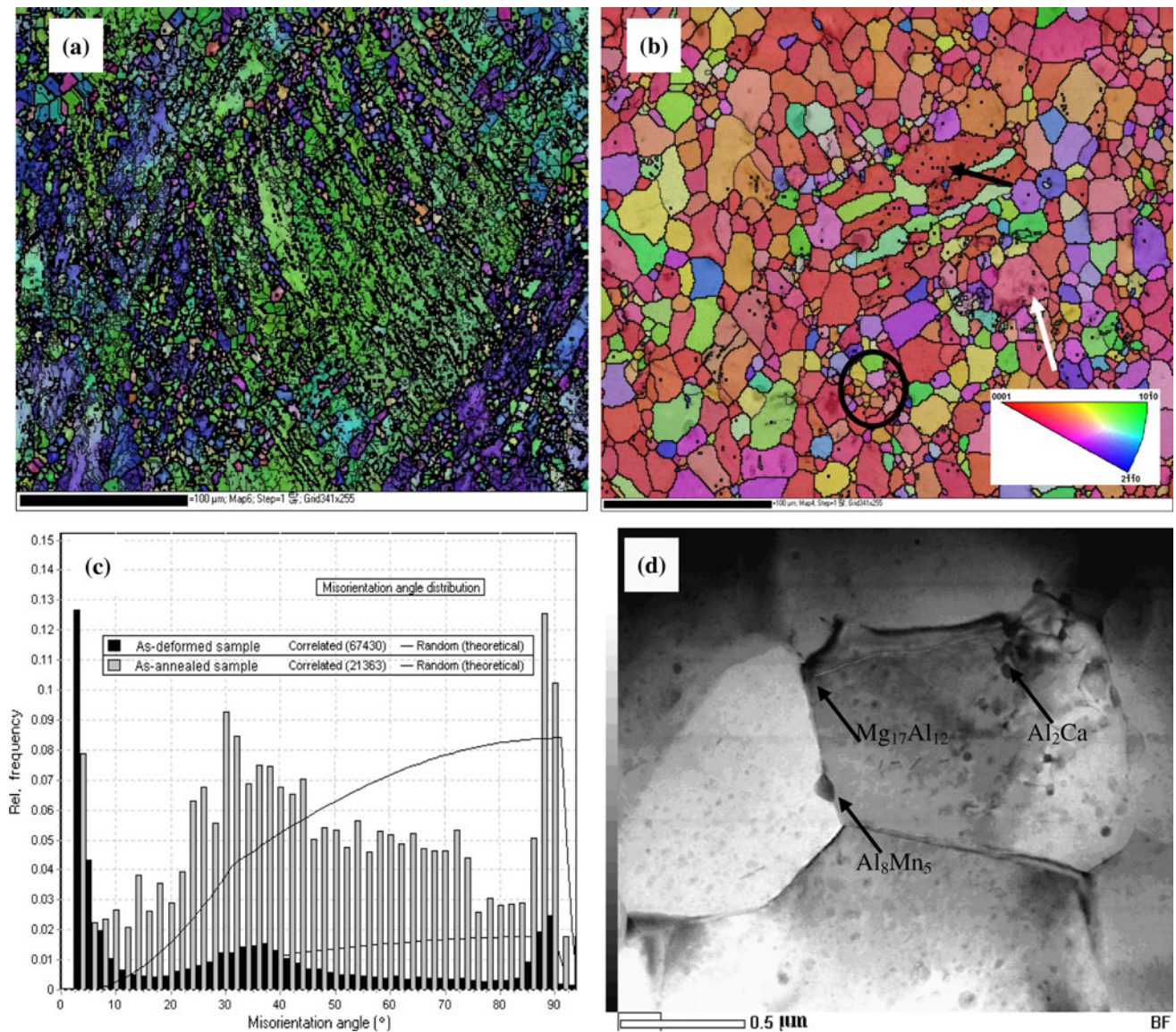


Fig. 2 **a** Orientation map of AZ41M alloy under deformed state of 300 °C/0.1 s⁻¹, **b** orientation map of AZ41M alloy under annealed conditions of 300 °C/1000 s, **c** misorientation angle in deformed and

annealed conditions, and **d** particles TEM micrograph under annealed conditions

The pinning forces is described as,

$$F = \frac{3}{2} \gamma r f \quad (3)$$

The grain-boundary energy of magnesium is reported to be 92 kJ/mol. The calculated grain size, volume fraction, driving force, and pinning forces are shown in Table 2. For large particles, $P \leq F$, Zener pinning effect is neglected, however, for fine particles, $P \geq F$, indicating that the inhibition effect of grain growth by a dispersed second phase is relatively effective. Precipitates result in the increases of dislocation density and alteration of slip homogeneity, finally cause the deformation heterogeneity (circle in Fig. 3a). However, the real microstructural

geometry of the particles is not neglected. It is known that the pinning force varies with particle shape such as ellipsoidal or cubic. This variation in pinning energy is due to the different amounts of missing boundary formed from intersection with particles of different shapes and orientations [12]. Form Fig. 3a, the grain boundary pinned by particles causing curvature of grain boundaries (CGB) (white arrow in Fig. 3a). CGB cumulation results in strain energy fluctuation producing a dislocation-free region behind the pinning particles. Fine particles retard dislocation glide forming high density dislocation regions. It is also observed that amount of fine particles are studded into the thick dislocation wall to drag the grain-boundary migration. These phenomena that DRX is prevented or

Table 2 Parameters value calculated from Eqs. 1, 2, and 3

	r (μm)	f (%)	γ (kJ/mol)	R (μm)	$P(\text{N})$	$F(\text{N})$
Large particles	2.0	4.1	92.0	65.0	2.83	67.3
Fine particles	0.6	8.9	92.0	8.9	20.7	9.3

delayed by a dispersions of closely spaced second-phase particles, due to the pinning (Zener drag), have been reported in the literature [11].

PSN is also often inferred to have occurred in wrought magnesium [13–15]. Annealing temperature increases which leads to the decrease of the amounts of LAGBs. Note that the HAGBs are dominant when the annealing temperature achieved to 300 °C (Fig. 3b). Form Fig. 3c, in the vicinity of large hard particles during deformation, a new HAGBs forms. The deformation zones around precipitate are preferred nucleation sites for recrystallization owing to the high dislocation density and high misorientation (arrow in Fig. 3c). That is, the region around the precipitates possessing a high dislocation density and large orientation gradient lead to form a new subgrain. However, for deformed sample, it appears that there is no clear

correlation between the recrystallized grains and second-phase particles. The real geometry size and distribution state of the particles have a distinctly effect on DRX. Literature [2] has reported that isolated coarse particles within the original grains, even those approaching 10 μm in diameter, did not lead to formation of DRX grains. In these studies, even the size of the isolated coarse particles is larger than 1 μm in diameter, DRX grains are not found in the vicinity of them (arrows in Fig. 4b). However, when the size of the isolated coarse particle approaches 2 μm , some new DRXed grains occur in the vicinity of particle by PSN (arrow in Fig. 4a). Clusters of particles are known to be more effective than single particles according to PSN. A cluster of coarse particles within a deformed grain certainly lead to classical PSN. That is, a particle cluster effectively acts like one very large particle. However, even though the size of a single particle in a cluster is small ($\leq 1 \mu\text{m}$), this particle cluster still results in PSN (ellipsoid in Fig. 3c).

Twinning is positive for promoting of DRX and SRX. The combined promotion of twin and particles result in rapidly formation of DRXed and SRXed grains. The activation of slip systems induces the formation of twin lamellae (Fig. 3d). The lamellar structure will tend to

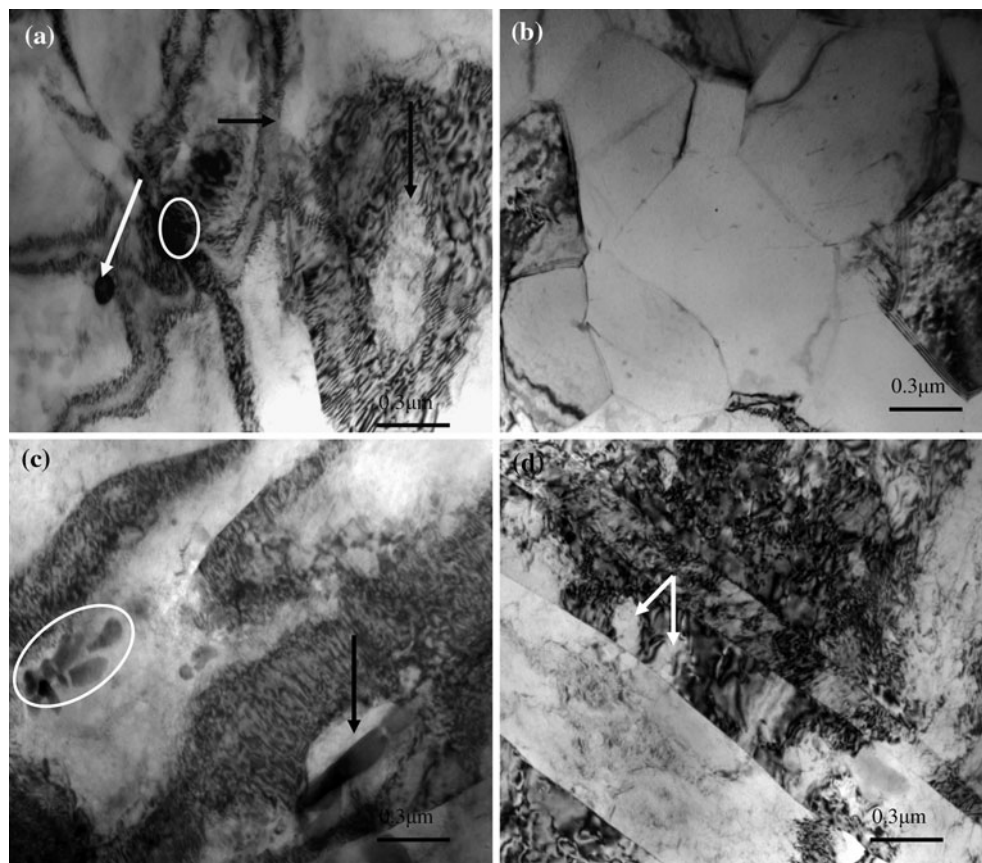
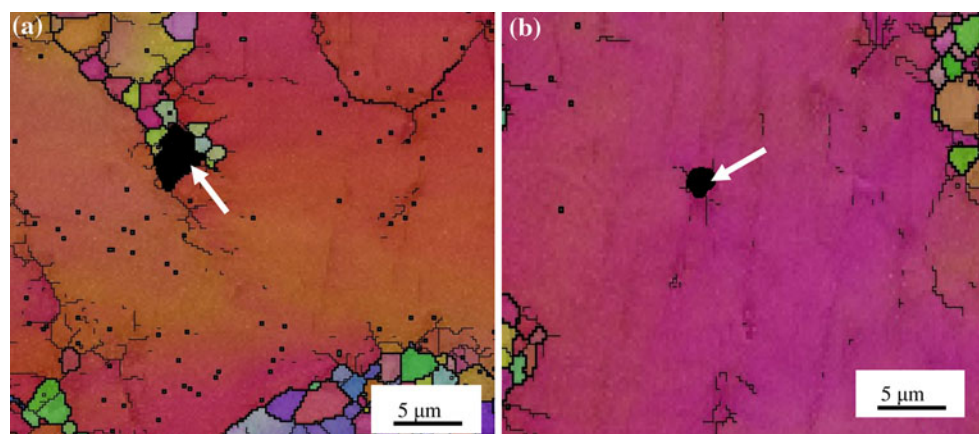


Fig. 3 **a** The increases of dislocation density forming dislocation wall result in the formation of subgrains embryo, **b** large PSN, **c** the dominant HAGBs, and **d** twins

Fig. 4 **a** Around isolated large particle ($\geq 2 \mu\text{m}$), new grains formed by PSN, **b** isolated particle ($< 2 \mu\text{m}$) has a minor effect on DRX



collapse due to the un-symmetrical distribution of dislocation and distribution of second-phase particles. So dislocation glides and piles up induce occurring of non-basal dislocation. Non-basal dislocation re-arrangement in the lamellae forms subgrains (arrow in Fig. 3d).

Conclusions

The grain-boundary migration mainly depends on the balance between the driving and the pinning forces. Fine particles retard dislocation glide forming high density dislocation. Amount of fine particles are studded into the thick dislocation wall to drag the grain-boundary migration. Large particles promote recrystallization. The real geometry size and distribution state of the particles have a distinctly effect on DRX. In the vicinity of large isolated particles ($\geq 2 \mu\text{m}$) during deformation, a new HAGBs forms. Clusters of particles are known to be more effective than single particles according to PSN. A cluster of fine particles ($< 1 \mu\text{m}$) still results in PSN.

Acknowledgements This study was supported by the Natural Science Foundation of Shandong Province (ZR2009FL003), the S&T Developing Program of Shandong Province, China (2010GGX10301).

and Science and Technology Development Project of Ministry of Education of Shandong (J10LD19).

References

- Buha J (2008) Mater Sci Eng A 492(1–2):293
- Robson JD, Henry DT, Davis B (2009) Acta Mater 57:2739
- Lee JY, Lim HK, Kim DH, Kim WT, Kim DH (2008) Mater Sci Eng A 491:349
- Mendis CL, Ohishi K, Kawamura Y, Honma T, Kamado S, Hono K (2009) Acta Mater 57(3):749
- Zarandi F, Sealea G, Vermab R, Essadiqi E, Yuea S (2008) Mater Sci Eng A 46:159
- Liu SF, Li B, Wang XH, Su W, Han H (2009) J Mater Process Tech 209–8:3999
- Wang QD, Chen WZ, Zeng XQ, Lu YZ, Ding WJ (2001) J Mater Sci 36:3035
- Park JP, Kim MG, Yoon US, Kim WJ (2009) J Mater Sci 44:47. doi:[10.1007/s10853-008-3130-z](https://doi.org/10.1007/s10853-008-3130-z)
- Xue F, Min XG, Sun YS (2006) J Mater Sci 41:4725. doi:[10.1007/s10853-006-0060-5](https://doi.org/10.1007/s10853-006-0060-5)
- Maazi N, Penelle R (2009) Mater Sci Eng A504:135
- Zener C (1948) TMS-AIME 175:15. Cited by CS. Smith
- Liu YX, Patterson BR (1996) Acta Mater 44:4327
- Beer AG, Barnett MR (2007) Metall Mater Trans A 38:1856
- Lorimer GW, Mackenzie LWF, Humphreys FJ, Wilks T (2005) Mater Sci Forum 448–489:99
- Hakamada M, Watazu A, Saito N, Iwasaki H (2008) J Mater Sci 43:2066. doi:[10.1007/s10853-008-2474-8](https://doi.org/10.1007/s10853-008-2474-8)